Available online at www.sciencedirect.com

SCIENCE DIRECT®

Geomorphology 63 (2004) 103–113

GEOMORPHOLOGY

www.elsevier.com/locate/geomorph

Comparison of aerodynamically and model-derived roughness lengths (z_o) over diverse surfaces, central Mojave Desert, California, USA

David J. MacKinnon[a,*], Gary D. Clow[b], Richard K. Tigges[b], Richard L. Reynolds[b], P.S. Chavez Jr.[a]

[a] *U.S. Geological Survey, 2255 N. Gemini Drive, Flagstaff, AZ 86001, USA*
[b] *U.S. Geological Survey, MS 980, Box 25046, Federal Center, Denver, CO 80225, USA*

Received 20 October 2002; received in revised form 30 March 2004; accepted 31 March 2004
Available online 2 July 2004

Abstract

The vulnerability of dryland surfaces to wind erosion depends importantly on the absence or the presence and character of surface roughness elements, such as plants, clasts, and topographic irregularities that diminish wind speed near the surface. A model for the friction velocity ratio has been developed to account for wind sheltering by many different types of co-existing roughness elements. Such conditions typify a monitored area in the central Mojave Desert, California, that experiences frequent sand movement and dust emission. Two additional models are used to convert the friction velocity ratio to the surface roughness length (z_o) for momentum. To calculate roughness lengths from these models, measurements were made at 11 sites within the monitored area to characterize the surface roughness element. Measurements included (1) the number of roughness species (e.g., plants, small-scale topography, clasts), and their associated heights and widths, (2) spacing among species, and (3) vegetation porosity (a measurement of the spatial distribution of woody elements of a plant). Documented or estimated values of drag coefficients for different species were included in the modeling. At these sites, wind-speed profiles were measured during periods of neutral atmospheric stability using three 9-m towers with three or four calibrated anemometers on each. Modeled roughness lengths show a close correspondence (correlation coefficient, 0.84–0.86) to the aerodynamically determined values at the field sites.

The geometric properties of the roughness elements in the model are amenable to measurement at much higher temporal and spatial resolutions using remote-sensing techniques than can be accomplished through laborious ground-based methods. A remote-sensing approach to acquire values of the modeled roughness length is particularly important for the development of linked surface/atmosphere wind-erosion models sensitive to climate variability and land-use changes in areas such as the southwestern United States, where surface roughness has large spatial and temporal variations.
© 2004 Elsevier B.V. All rights reserved.

Keywords: Aerodynamic roughness; Boundary layer; Wind erosion; Deflation; Desertification processes

* Corresponding author.

0169-555X/$ - see front matter © 2004 Elsevier B.V. All rights reserved.
doi:10.1016/j.geomorph.2004.03.009

1. Introduction

Surfaces most responsive to wind erosion are nearly flat, contain loose sand-sized particles, and lack objects (roughness elements that are non-erodible by the wind) that would otherwise shelter or cover the surface. On such surfaces, the threshold wind stress, at which erosion begins, depends only on the median diameter of the loose sand-sized particles on the surface (Greeley and Iversen, 1985). This rather simple relation becomes far more complex for most natural surfaces having non-erodible roughness elements, such as small-scale topographic irregularities, clasts (rocks greater than 1 mm in diameter), and plants. In the presence of these roughness elements, the threshold wind stress can be much greater than that for a barren surface (Musick et al., 1996). The quantitative role of these non-erodible elements in sheltering the surface against wind erosion is the subject of ongoing research. Relatively recent studies by Raupach (1992), Raupach et al. (1993), and Marticorena et al. (1997), in particular, have derived mathematical expressions for the threshold wind stress and for the related surface roughness length in terms of height, width, spacing, and wind-drag properties of the non-erodible elements. Raupach (1994) proposed a much more simplified model than Raupach et al. (1993) for the wind field near the ground in sufficiently dense vegetation. Here the dense sheltering "displaces" the wind field upward to eliminate contact with the ground surface and any subsequent wind erosion. In this paper, we only consider relatively low roughness densities, typical of wind erosion areas, where the wind field reaches the ground and the partial sheltering effects of vegetation and other forms of roughness can be described by both Raupach et al.'s (1993) physical roughness model and Raupach (1992) and Marticorena et al.'s (1997) model of the surface roughness length.

The Raupach et al. (1993) algorithm that links the threshold wind stress to dimensionless surface roughness parameters applies to only a single roughness species (such as one plant type) residing on a bare surface. Their algorithm, therefore, is not fully applicable to surfaces that are covered by two or more different types (species) of roughness, as is common in many dryland areas susceptible to wind erosion. The algorithms of Raupach (1992) and Marticorena et al. (1997) that link the threshold wind stress to the surface roughness length apply only to a cover of limited extent.

This paper expands the roughness model of Raupach et al. (1993) to account for surfaces covered by many different types of non-erodible roughness elements, and it modifies an algorithm parameter of Marticorena et al. (1997) to account for the high aerodynamically determined roughness lengths measured at some of our field sites. These changes are then combined into a new model that derives the surface roughness length in terms of the properties of the non-erodible elements. Finally, the model-derived roughness lengths are compared to the aerodynamically determined roughness lengths for 11 field sites in the central Mojave Desert as a validation test. This new roughness model will become part of a wind-erosion model accounting for complex distributions of surface roughness that may change in response to climate variability (Lancaster, 1997).

2. Background: roughness models and their role in wind-erosion models

The new roughness model uses traditional terms to describe the shear stress (τ) imposed by the wind on the surface in terms of air density (ρ), wind speed (U), atmospheric stability, and the momentum roughness length z_{om}. Within the "surface sublayer" (i.e., the fully turbulent region within the atmospheric boundary layer (ABL) where turbulence production by wind shear exceeds that due to buoyancy), the wind stress is given by

$$\tau = \rho \left[\frac{U(z)}{F_{\mathrm{m}}(z_{\mathrm{om}}, z)} \right]^2, \tag{1}$$

where F_{m} is the integral momentum function defined by

$$F_{\mathrm{m}}(z_{\mathrm{om}}, z) = \int_{z_{\mathrm{om}}}^{z} \frac{\phi_{\mathrm{m}}(z)}{kz} \mathrm{d}z. \tag{2}$$

The form of the similarity-based dimensionless velocity gradient ϕ_{m} depends on atmospheric stability,

and thus is normally expressed in terms of the Monin–Obukhov stability parameter $\zeta=(z/L)$,

$$\phi_m(\zeta) = \begin{cases} 1+\beta_m\zeta & (\zeta \geq 0) \\ (1-\gamma_m\zeta)^{-1/4} & (\zeta < 0) \end{cases} \quad (3)$$

(Yaglom, 1997); L is the Monin–Obukhov length. Field experiments provide values for the parameterization constants. For example, Businger et al. (1971) found $\beta_m=4.7$, $\gamma_m=15$, and $k=0.35$. In terms of the stability parameter ζ, F_m can be expressed as

$$F_m(\zeta_{om},\zeta) = \frac{1}{k}\int_{\zeta_{om}}^{\zeta}\frac{\phi_m(\zeta)}{\zeta}\,d\zeta, \quad (4)$$

where $\zeta_{om}=(z_{om}/L)$. Substituting the functional form of ϕ_m into Eq. (4), the momentum function becomes

$$F_m(\zeta_{om},\zeta) = \begin{cases} \frac{1}{k}\left[\ln\left(\frac{\zeta}{\zeta_{om}}\right)+\beta_m(\zeta-\zeta_{om})\right] & \zeta>0 \\ \frac{1}{k}\left[\ln\left(\frac{\zeta}{\zeta_{om}}\right)\right] & \zeta=0 \\ \frac{1}{k}\left[\ln\left(\frac{\zeta}{\zeta_{om}}\right)+\ln\frac{(\psi_{om}^2+1)(\psi_{om}+1)^2}{(\psi_m^2+1)(\psi_m+1)^2}+2[\arctan(\psi_m)-\arctan(\psi_{om})]\right] & \zeta<0 \end{cases} \quad (5)$$

where $\psi_m=(1-\gamma_m\zeta)^{-1/4}$ and $\psi_{om}=(1-\gamma_m\zeta_{om})^{-1/4}$. Returning to Eq. (1), the dependence of the surface wind stress on the surface roughness (described by parameter z_{om}, or ζ_{om}) is embodied in the integral momentum function F_m. The familiar scaling velocity u (i.e., "friction" velocity) is given by,

$$u_* = \frac{U(z)}{F_m(z_{om},z)}, \quad (6)$$

revealing its dependence on the momentum roughness length z_{om} through F_m. With this definition, the wind stress can be written simply as $\tau=\rho u_*^2$.

The above relations are valid for both aerodynamically smooth and aerodynamically rough surfaces. However, the focus of this paper is on aerodynamically rough surfaces, for which the viscous length scale (ν/u_*) is much less than the momentum roughness length, z_{om}. By convention, the momentum roughness length for rough airflow is also known as the "surface roughness length", z_o.

The roughness length has two roles in wind-erosion models. First, the threshold wind stress at which eolian erosion begins depends on z_o (e.g., Marticorena et al., 1997). Second, the free-stream wind field above the ABL is driven by regional pressure gradients that evolve over time by well-known atmospheric equations of motion. Within the ABL, the wind field is a result of the complex transfer of free-stream wind momentum downward to overcome the drag caused by the non-erodible roughness elements, and depends on regional atmospheric dynamics, atmospheric stability, topography at local and regional scales, and on the surface roughness length z_o (Grell et al., 1995). Thus, the roughness length has an important feedback on the wind field and associated surface stress. This feedback is important, because wind-erosion rates depend on the amount that the wind stress exceeds the threshold value at which erosion occurs (Gillette, 1988). Therefore, roughness models play a critical dual role in wind-erosion modeling by affecting both the shear stress imposed by the wind on the surface as well as the threshold stress at which erosion initiates.

2.1. Aerodynamically derived surface roughness length, z_o^A

The traditional method for calculating the aerodynamically derived roughness length z_o^A is based on wind-speed measurements during thermally neutral atmospheric conditions, $\zeta=0$ (Brutsaert, 1982). Superscripts A and M are used here to distinguish aerodynamically derived and model-derived values for z_o. The aerodynamic roughness z_o^A is obtained from a least-squares fit to the wind-speed measurements made simultaneously at three or more heights within the dynamic portion of the surface sublayer where winds generally maintain a logarithmic profile; z_o^A is defined to be the height above the surface at which the wind speed would drop to zero if the logarithmic profile is extrapolated down into the interfacial sublayer. Under thermally neutral conditions, the roughness length is also a characteristic measure of the drag on the wind field caused by non-erodible roughness elements: z_o^A increases in proportion to the size, spacing, and drag properties of these elements. Many researchers have used the aerodynamically derived roughness length to characterize the excess momentum extracted from the wind field by upwind roughness elements (e.g., Brutsaert, 1982; Lee, 1990; Wolfe, 1993; Wolfe and Nickling, 1996).

The aerodynamically derived roughness length may not be a reliable measure of the effects of surface roughness under all conditions. In some field experiments, winds are suddenly displaced upward (displacement height) in a manner that may not be explained by roughness length alone (Brutsaert, 1982; Lee, 1990). In such cases, typically characterized by dense stands of vegetation, the wind stress no longer reaches the surface. Therefore, the use of a surface roughness length as a measure of the drag imposed by the surface roughness elements becomes invalid.

Within the porous canopies typical of desert flora, Wolfe (1993) found, however, that wind passes through all roughness elements and may contact the surface. Because the bare surface still extracts momentum in an environment covered by porous roughness elements, the surface roughness length can increase to very large values before all wind stress is prevented from affecting the bare surface. At high roughness densities for porous roughness elements, the wind profile does not show an abrupt displacement upward. Wind data collected by Lee (1990) in deserts with porous vegetation were re-evaluated by Wolfe (1993) to show that the data better fit a wind-profile model without a zero-plane displacement height and with rather large roughness lengths (as much as 3.8 cm). Wolfe (1993) aerodynamically derived values of roughness length substantially exceed the largest values (0.6 cm) reported by Marticorena et al. (1997). Wolfe's results are consistent with the largest roughness lengths (as much as 7.1 cm) measured at some of the sites reported in this paper.

2.2. Model-derived roughness length, z_o^M

A useful concept in modeling surface roughness lengths is the "efficient friction velocity ratio", f_{eff}, defined by Marticorena et al. (1997) as the ratio of the threshold friction velocity of a bare surface $u_{*\mathrm{ts}}$ to the threshold friction velocity of a surface covered by non-erodible roughness elements, $u_{*\mathrm{t}}$. Marticorena et al. (1997) showed that $f_{\mathrm{eff}}[\equiv(u_{*\mathrm{ts}}/u_{*\mathrm{t}})]$ depends primarily on the amount that the roughness length $z_{\mathrm{o}}^{\mathrm{M}}$ for a covered surface exceeds the roughness length of a bare surface $z_{\mathrm{os}}^{\mathrm{M}}$. In this way, sheltering of a surface (expressed as a ratio of threshold friction velocities) can be expressed in terms of covered- and barren-surface roughness lengths, $f_{\mathrm{eff}} \equiv f_{\mathrm{eff}}(z_{\mathrm{o}}^{\mathrm{M}}, z_{\mathrm{os}}^{\mathrm{M}})$.

Marticorena et al. (1997) also showed that their efficient friction velocity ratio f_{eff} is equivalent to the "friction velocity ratio" $R_{\mathrm{t}} \equiv (u_{*\mathrm{ts}}/u_{*\mathrm{t}})$ defined by Raupach et al. (1993). This is an important relation, because Raupach et al. (1993) derived R_{t} in terms of measurable height, width, separation, and drag-coefficient parameters for a single species of roughness elements on a bare surface. The equivalence of f_{eff} and R_{t} provides a connection between the measurable roughness quantities and $z_{\mathrm{o}}^{\mathrm{M}}$.

3. Modification and linking of roughness models: theory and methods

The approach in this paper makes use of the algorithms of Raupach (1992), Raupach et al. (1993) and Marticorena et al. (1997) to determine model-derived values of the surface roughness length $z_{\mathrm{o}}^{\mathrm{M}}$ in terms of the properties of the roughness elements. By modifying the algorithm of Raupach et al. (1993), we are able to consider surfaces consisting of multiple species of roughness elements. Roughness features are assigned to a particular species or group based on similarities in mean height, width, mutual separation, and drag coefficient. Differences between species reflect different plant types or different surface components (e.g., clasts or dirt mounds).

We also modify a parameter in Marticorena et al. (1997; Eq. (9), p. 23280) f_{eff} algorithm to accommodate evidence for high roughness length values in porous vegetation (Wolfe, 1993; this study).

3.1. Stress partitioning among multiple roughness species

Stress partitioning on one species of many individual roughness elements lying on a bare surface, developed by Raupach et al. (1993), was expanded to incorporate stress partitioning among multiple species of many, individual roughness elements. The first aspect of the expansion involves the total wind stress τ_{t} imposed on the surface, which we consider to be a sum of the wind stress experienced by each roughness species above the surface (τ_{R1},

τ_{R2}, …, τ_{Rn}) plus the stress experienced by the surface itself τ_s,

$$\tau_t = \tau_s + \sum_{i=1}^{n} \tau_{Ri}. \quad (7)$$

The surface stress τ_s is related to the stress on the bare (exposed) surface τ_s' by,

$$\tau_s = \left(1 - \sum_{i=1}^{n} \sigma_i \lambda_i\right) \tau_s' \quad (8)$$

where $\sigma_i\lambda_i$ is the fraction of basal area covered by species i; the dimensionless roughness parameters σ, λ, β are formally defined in the next section. The ratio of the shear-stress on an individual roughness species to the total shearing stress for n roughness species (derived by analogy to Eq. (7) of Raupach et al., 1993, p. 3025) is

$$\frac{\tau_{Ri}}{\tau_t} = \left(\frac{\beta_i \lambda_i}{1 + \sum_{i=1}^{n} \beta_i \lambda_i}\right), \quad (9)$$

where $\beta_i\lambda_i$ is the total non-dimensional shear stress on species i per unit surface area. The "1" in the denominator on the right-hand side of Eq. (9) results from the ratio of the total non-dimensional shearing stress on the surface (considered similar to a species of roughness) per unit surface area being equal to 1.

Denoting the threshold friction velocity of a bare surface by u_{*ts}', we define $R_t \equiv (u_{*ts}'/u_t)$, or equivalently $R_t = \sqrt{\tau_s'/\tau_t}$ since $u_* = \tau/\rho$. Utilizing Eqs. (7)–(9), R_t can be expressed in terms of the roughness parameters σ_i, λ_i, β_i for the n species,

$$R_t = \left[\left(1 - \sum_{i=1}^{n} m_i \sigma_i \lambda_i\right)\left(1 \sum_{i=1}^{n} m_i \beta_i \lambda_i\right)\right]^{-1/2}. \quad (10)$$

An additional parameter m_i is included to account for the non-uniformity of surface wind stress around the roughness elements species. Eq. (10) reduces to Eq. (11) below of Raupach et al. (1993, p. 3025) when there is only one roughness species (i) on the bare surface.

$$R_i = [(1 - m_i\sigma_i\lambda_i)(1 + m_i\beta_i\lambda_i)]^{-1/2}. \quad (11)$$

Eq. 10 can be rewritten in terms of Eq. (11) by first inverting and squaring Eq. (10) and second by noting that for most common situations $m_i\sigma_i\lambda_i \ll 1$ in Eq. (11) and more generally $\sum_{i=1}^{n} m_i\sigma_i\lambda_i \ll 1$ in Eq. (10). The latter follows because $\sum_{i=1}^{n} \sigma_i\lambda_i$ (Eq. (6)), the fraction of surface area covered by all roughness species, is typically much less than one for stress partitioning to apply. Setting $m_i\sigma_i\lambda_i \approx 0$, expanding the r.h.s. of Eq. (10) and collecting terms similar to Eq. (11) yields

$$\frac{1}{R_t^2} \approx \sum_{i=1}^{n} \frac{1}{R_i^2} - (n-1) \quad (12)$$

This approximation is useful for assessing the contribution of each roughness species to the total threshold friction velocity ratio R_t. (By expanding all terms in Eq. (10), it can be shown that Eq. (12) remains valid under the less restrictive conditions of $m_i\sigma_i\lambda_i \ll 1$ instead of $\sum_{i=1}^{n} m_i\sigma_i\lambda_i \ll 1$.

3.2. Parameterization of expanded theory for application to field data

In order to use Eqs. (10) and (11) to model the roughness length z_o, we must define the roughness-element parameters σ, λ, β, and m for each species in terms of the roughness-element height h, width w, mutual separation D between roughness elements of the same species, and the drag coefficient C_d, and then establish an equation that relates R_t to z_o^M (the modeled roughness length). Following Raupach et al. (1993), the dimensionless roughness parameters for the ith species are:

$$\sigma_i \equiv \left(\frac{\text{basal area}}{\text{frontal area}}\right)_i = \frac{w_{i1} w_{i2}}{w_i h_i} \quad (13)$$

$$\lambda_i \equiv \left(\frac{\text{frontal area}}{\text{associated ground area}}\right)_i = \frac{\pi w_i h_i}{4 D_i^2}, \text{ and} \quad (14)$$

$$\beta_i \equiv \frac{C_{d_i}}{C_{d_s}}, \quad (15)$$

where w_{i1} and w_{i2} are two orthogonal width measurements across a roughness element, w_i is the average of these two widths, and C_{d_s} is the drag coefficient for a bare surface. Raupach (1992) and Raupach et al.

(1993) found C_{d_s} to be between 0.0018 and 0.003 in their study. However, we use C_{d_s}, which is consistent with the field data of Wyatt and Nickling (1997) and bounded by the former results. Finally,

$$0.16 \leq m \leq 1.0, \tag{16}$$

where m is near 1.0 for solid objects and decreases as porosity increases. In this paper (see Table 1) we estimated values of m and C_{d_i} based on published values from Raupach (1992), Raupach et al. (1993), Wyatt and Nickling (1997), and Grant and Nickling (1998). The estimated values considered that as m approaches 0.16, C_{d_i} approaches 0.6 for porous vegetation, and that as m approaches 1.0, C_{d_i} approaches 0.2–0.3 (values for sphere/cylinder) for solid objects or very dense vegetation. Cubes with sharp edges have a drag coefficient near 0.4. Recent results

Table 1
Mean and standard deviation values of measured height (h, s_h), width (w, s_w), and separation (D, s_D), estimated non-uniformity of wind stress (m, s_m), drag coefficient (C_d, s_{C_d}), and calculated roughness parameters (σ, λ, β, R_i) for observed roughness types (species) at each of 11 field sites

Site #	*R*-type	h	s_h	w	s_w	D	s_D	m	s_m	C_d	s_{C_d}	σ	λ	β	R_i
200–201	annuals	0.3	0.05	0.5	0.1	0.5	0.2	0.2	0.005	0.59	0.1	1.67	0.47	246	0.22
	coppice	0.45	0.15	0.3	0.1	5	0.2	0.5	0.1	0.3	0.05	0.67	0.004	125	0.89
	hfrough	0.2	0.1	0.5	0.1	4.0	0.1	0.8	0.1	0.4	0.05	2.5	0.005	167	0.78
202	creosote	1.7	0.35	2.3	0.62	9.7	1.7	0.16	0.005	0.69	0.1	1.35	0.03	288	0.64
	annuals	0.1	0.05	0.1	0.05	0.5	0.1	0.2	0.005	0.59	0.1	1.0	0.03	246	0.63
	hfrough	0.2	0.1	0.5	0.1	4.0	0.1	0.8	0.1	0.4	0.05	2.5	0.004	167	0.78
203	creosote	1.3	0.41	2.3	0.57	12.0	2.8	0.16	0.005	0.69	0.1	1.77	0.015	288	0.77
	annuals	0.09	0.02	0.1	0.05	0.75	0.25	0.2	0.005	0.59	0.1	1.18	0.012	246	0.80
	hfrough	0.2	0.1	0.5	0.1	4.0	0.1	0.8	0.1	0.4	0.05	2.5	0.005	167	0.78
204	succlnt	0.7	0.19	0.71	0.17	2.8	0.62	0.3	0.1	0.59	0.05	1.01	0.052	246	0.46
	annuals	*	*	*	*	*	*	*	*	*	*	*	*	*	*
	coppice	0.4	0.2	0.5	0.05	2.5	0.5	0.5	0.1	0.3	0.05	1.25	0.025	125	0.63
205	creosote	1.3	0.25	1.4	0.33	6.6	2.0	0.16	0.005	0.69	0.1	1.08	0.033	288	0.63
	borage	0.2	0.05	0.1	0.005	0.2	0.005	0.3	0.1	0.4	0.1	0.5	0.393	167	0.23
206	hilaria	0.71	0.1	0.77	0.21	1.9	0.47	0.3	0.1	0.59	0.1	1.09	0.116	246	0.33
	coppice	0.5	0.1	0.77	0.21	1.9	0.47	0.5	0.1	0.3	0.05	1.53	0.082	125	0.42
207	creosote	1.4	0.28	1.9	0.39	9.3	3.7	0.16	0.005	0.69	0.1	1.31	0.024	288	0.69
	bursage	0.48	0.12	0.71	0.26	2.8	1.2	0.7	0.1	0.5	0.1	1.47	0.033	208	0.42
	rocklag	0.01	0.001	0.01	0.001	0.05	0.005	0.8	0.1	0.4	0.1	1.0	0.031	167	0.44
208	unkbush	0.8	0.2	1.1	0.39	30.0	0.2	0.3	0.1	0.5	0.05	1.38	0.0008	208	0.98
	coppice	0.3	0.1	1.0	0.1	30.0	1.0	0.5	0.1	0.3	0.05	2.33	0.0003	125	0.99
	saltpush	0.02	0.005	0.1	0.005	0.5	0.1	0.8	0.1	0.4	0.05	5.0	0.006	167	0.75
209	unkbush	0.55	0.17	0.96	0.43	3.3	1.2	0.3	0.1	0.5	0.05	1.74	0.039	208	0.55
	coppice	0.4	0.1	0.5	0.1	5	0.2	0.5	0.1	0.3	0.05	1.25	0.0062	125	0.85
	annuals	0.2	0.1	0.1	0.005	0.5	0.1	0.8	0.1	0.59	0.05	0.5	0.062	246	0.28
210	creosote	1.7	0.418	2.6	0.72	7.5	3.1	0.16	0.005	0.69	0.1	1.52	0.062	288	0.51
	unkbush	0.6	0.105	0.9	0.22	3.1	1.3	0.3	0.1	0.5	0.05	1.50	0.044	208	0.52
	coppice	0.8	0.2	0.8	0.2	3.0	0.2	0.5	0.1	0.3	0.05	1.0	0.056	125	0.48
211	unkbush	0.83	0.206	1.7	0.59	6.1	2.5	0.5	0.1	0.5	0.05	2.02	0.029	208	0.47
	coppice	0.26	0.086	1.5	0.2	5.0	1.3	0.5	0.1	0.3	0.05	5.77	0.012	125	0.48

All geometric parameters are measured in meters. R_i (Eq. (11) in the text) is the model-derived, threshold friction velocity ratio for each roughness type as listed in the second column (*R*-type); a smaller value of R_i denotes a higher sheltering effect. Roughness types are as follows: *annuals*—a non-specific collection of weeds, flowers, and grasses that depend on yearly rainfall; *coppice*—dunes accumulating under living and dead plant communities; *hfrough*—high-frequency, topographic roughness elements larger than sand ripples but smaller than coppice dunes; *creosote*—the common creosote bush; *succlnt*—bush species whose dormant and active leaf and stem components are composed of a high percentage of water compared to the components of more woody species, such as creosote; *borage*—a low-height annual plant; *bursage*—a medium-height bush common to the Mojave Desert; *hilaria*—a tall perennial grass; *unkbush*—an unknown bush; *rocklag*—a distribution of surface clasts that armor the surface; *saltpush*—salt push-ups or ridges created by expanding salt and clay crusts on playa surfaces. At site 204, the roughness properties of the annual plants were not measured.

(Crawley and Nickling, 2003) derived values of m for regularly arrayed solid roughness elements between 0.53 and 0.58 which are consistent with those used in our estimation scheme.

Using Eqs. (5) and (6) for neutral atmospheric thermal conditions ($\zeta = 0$), the result is the well-known inertial-sublayer logarithmic law, which describes the wind profile at height ($z = h$) equal to the tallest roughness element according to

$$\frac{U(h)}{u_*} = F_m(z_{om}, h) = \frac{1}{k}\ln\left\{\frac{h}{z_o^M}\right\}, \quad (17)$$

where $z_{om} = z_o^M$ (for notation consistency with Marticorena et al., 1997) is the modeled momentum roughness length for a bare surface covered with roughness elements. Eq. (17) is similar to Raupach (1992; 1994) with the additional assumptions that there is no displacement height in the wind profile ($d = 0$ in Raupach, 1992, Eq. (27); 1994, Eq. (4)) and that there is no variation in the form of the logarithmic law just above the inertial sublayer at height h of the tallest roughness species ($\psi_h = 0$ in Raupach, 1992, Eq. (27); 1994, Eq. (4)). The former condition appears valid for sparsely leafed desert vegetation (Wolfe, 1993), and the latter condition may also be valid because the sparse vegetation diffuses the momentum deficit gradually through the canopy and does not create sharp wake boundaries.

Raupach (1992, Eq. (27); 1994, Eq. (4)) showed that the left-hand side of our Eq. (17) can be written in terms of the total stress, which is our Eq. (7), without strong mutual sheltering among the roughness elements, as

$$\frac{U(h)}{u_*} = \frac{1}{C_{d_s}^{1/2}\left(1 + \sum_{i=1}^{n} m_i\beta_i\lambda_i\right)^{1/2}} \approx \frac{R_t}{C_{d_s}^{1/2}} \quad (18)$$

where the right-hand side of Eq. (18) follows from our Eqs. (10) and (11) with the condition that for our data (see Table 1) $\sum_{i=1}^{n} m_i\sigma_i\lambda_i \ll 1$. Noting that, as $\lambda_i \to 0$, the surface becomes bare of roughness elements, so that $z_o^M \to z_{os}^M$ in our Eq. (17) and noting that, as $R_t \to 1$, so that $u_* \to u_{*_s}$ in our Eq. (18). Combining these changes, Eq. (17) can be rewritten as,

$$R_t \equiv \left(\frac{u_{*_{ts}}'}{u_{*_t}}\right) = \left(\frac{u_{*_s}}{u_*}\right) = 1 - \left\{\ln\left(\frac{z_o^M}{z_{os}^M}\right) \Big/ \ln\left(\frac{h}{z_{os}^M}\right)\right\}. \quad (19)$$

Marticorena et al. (1997) developed a relation similar to our Eq. (19) but argued for another length-scale dependency. Field tests of threshold wind speeds on soils devoid of plants and other large-scale roughness elements illustrate the importance of small-scale topographic irregularities and particles on the surface, either as aggregates of soil particles or rock fragments as large as gravel (Marticorena et al., 1997). The irregularities and particles shelter the surface against wind erosion, creating a large increase in threshold friction velocity as the surface roughness increases. Based on wind-profile matching arguments between and above the largest roughness elements, Marticorena et al. (1997) propose that the ratio of the bare-surface friction velocity to the total friction velocity is,

$$f_{eff} \equiv \left(\frac{u_{*_s}}{u_*}\right) = 1 - \left\{\ln\left(\frac{z_o^M}{z_{os}^M}\right) \Big/ \ln\left[\alpha\left(\frac{x}{z_{os}^M}\right)^p\right]\right\}. \quad (20)$$

This relation assumes that a logarithmic wind profile develops between roughness elements that are not too closely spaced. Both field experiments and wind tunnel measurements indicate $\alpha \approx 0.35$ and $p \approx 0.8$ for a wide range of surface roughness conditions. Marticorena et al. (1997) suggested that the validity of Eq. (17) is probably limited to roughness densities $\lambda < 0.05$ (Arya, 1975).

Marticorena et al. (1997) found that the effective friction velocity ratio f_{eff} is insensitive to the parameter x (roughness factor) in Eq. (20). At least for their study area (Chihauhaun Desert, southwestern USA), the best agreement with their data occurs with $x = 10$ cm. Eq. (20) is plotted for this value of x (solid curve) in Fig. 1 along with measurements (+) by Marticorena et al. (1997). The plots show that, for the same roughness length z_o^M, surfaces of clay or biologic crusts have much higher threshold friction velocities than surfaces of loose or disrupted

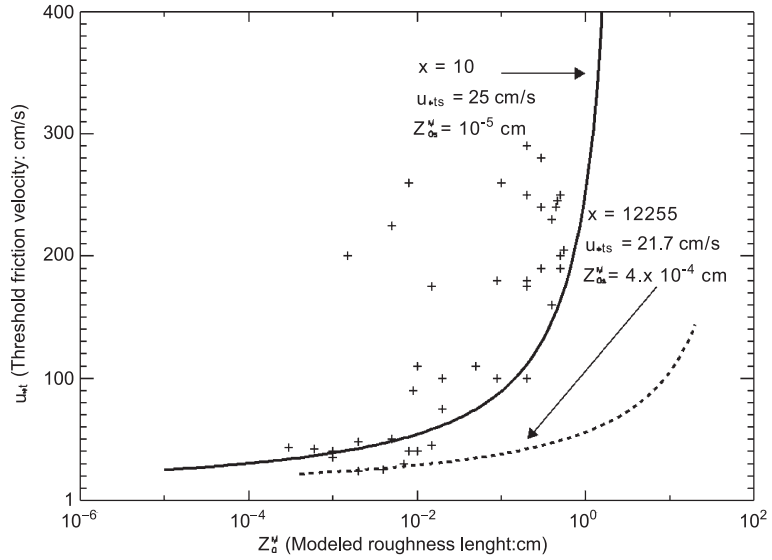

Fig. 1. Comparison of u_{*t} as a function of model-derived roughness length (z_o^M) for some of Marticorena et al. (1997; Fig. 1 and Fig. 2, p. 23,281 and p. 23,282, respectively) data (+). Not all data points are plotted, but the Marticorena data did not exceed $z_o^M \approx 0.6$ cm. The solid curve is plotted using Eq. (17) with $x = 10$, u_{*ts} 25 cm/s, and $z_{os}^M = 10^{-5}$ cm; the dashed curve is plotted with $x = 12{,}255$, $u_{*ts} = 21.7$ cm/s, and $z_{os}^M = 4 \times 10^{-4}$ cm.

materials. For these results the threshold friction velocity is

$$u_{*t}(z_o^M, z_{os}^M) = \frac{u_{*ts}}{f_{eff}(z_o^M, z_{os}^M)}. \quad (21)$$

Parameter x is tied to the height of the internal boundary layer between the roughness elements and thus may scale with the overall surface roughness. The largest value of z_o^M considered in the Marticorena et al. (1997) study was about 0.2 cm. Their results and value of x do not explain findings by Wolfe (1993) that sparsely leafed desert vegetation efficiently extracts wind momentum without creating significant wake eddies (p. 155) and maintains a logarithmic wind profile at least to roughness densities $\lambda \approx 0.5$ (p. 96) and roughness lengths to 3.81 cm (p. 162), similar to our results. Raupach et al. (1993) also showed that their model for R_t, the "threshold friction velocity ratio", explains a broad range of experimental data at roughness densities at least to $\lambda \approx 0.5$. These results suggest that $f_{eff} \equiv R_t$ may apply over a greater range of conditions than suggested by Marticorena et al. (1997).

In order to accommodate rougher surface conditions than found by Marticorena et al. (1997), we chose a lower and upper bound of corresponding threshold friction velocities and roughness lengths that would encompass both our and Marticorena et al.'s (1997) data (we chose this approach, because it is uncertain how parameter x in Eq. (20) scales with roughness element properties). For the lower bound, we chose bare surface values for the threshold friction velocity ($u_{*ts} = 21.7$ cm s^{-1}) and the roughness length ($z_{os}^M = 4 \times 10^{-5}$ cm), as calculated by Marticorena et al. (1997) model, for the most erodible particle sizes (60–120 μm in diameter). For the upper bound, we chose the threshold friction velocity at a roughness length of $z_o^M = 10$ cm to be $u_{*t} = 100$ cm s^{-1}. When placed into Eq. (17), these values yield a value of $x = 12{,}255$. Our choice of u_{*t} (approximately five times larger than u_{*ts} (21.7 cm s^{-1})) yields a value $f_{eff} = 0.2$ at $z_o^M = 10$ cm in Eq. (17). At f_{eff}, a natural surface would be largely sheltered against significant erosion (Raupach et al., 1993; p. 3027). These results are plotted as the dashed curve in Fig. 1.

Wind-drag conditions at our Mojave Desert sites imply that $f_{eff} \equiv R_t$, but the implication cannot be tested further, because we cannot be certain that this relation applies to our data. It is important to note, however, the similarity in form between Eq. (19)

(Raupach, 1992) and Eq. (20) (Marticorena et al., 1997) also lends support to the implication that $f_{\text{eff}} \equiv R_{\text{t}}$.

4. Discussion and conclusions

The aerodynamically derived (z_{o}^{A}) and model-derived (z_{o}^{M}) mean roughness lengths show a close correspondence over a range of three orders of magnitude (Table 2). A parametric test of this correspondence is the linear cross-correlation coefficients for the mean roughness lengths between sets of mean-value data in the three columns of Table 2. For this test, the logarithmic skewness and large dynamic range are first removed by taking the logarithm of the mean-value data and then the cross-correlation coefficients are derived. The cross-correlation coefficient result of the mean-value data between the aerodynamic and the Raupach models is 0.86, between the aerodynamic and the Marticorena models is 0.84, and between the Raupach and Marticorena models is 0.99.

A non-parametric test of the correspondence is the Mann–Whitney *U*-Test (or Wilcoxian Rank-Sum Test) where the null hypothesis is that the data in each column in Table 2 come from the same probability distribution (Conover, 1971). To reject the null hypothesis at the 5% significance level (or equivalently to accept the null hypothesis at the 95% significance level), the calculated *T*-statistic for the mean-value data columns in Table 2 would have to be less than 27 or greater than 104. The calculated *T*-statistic of the mean-value data between the aerodynamic and the Raupach model is 65.5, between the aerodynamic and the Marticorena model is 61.0, and between the Raupach and Marticorena models is 53.0. A hypothetical model that had perfect correspondence to the aerodynamic model would have a calculated *T*-statistic of 55.5. In all cases, it can be assumed to a high degree of confidence that the distributions of the mean-value data in Table 2 come from the same probability distribution, or that the Raupach and Marticorena models are good representations of the aerodynamic field data.

The high cross-correlation coefficient between the Raupach and Marticorena models suggests that either could be used to represent the aerodynamic field data, but the Raupach model is more straightforward and reflective of its dependence on roughness-element geometry. On the one hand, it is not clear that using

Table 2
Comparison of mean aerodynamic (z_{o}^{A}) and model-derived (z_{o}^{M}) surface roughness lengths for each site

Site #	Aerodynamic z_{o}^{A} (cm)		Raupach model z_{o}^{M} (cm)		Marticorena model z_{o}^{M} (cm)	
	Mean	Range	Mean	Range	Mean	Range
200–201	2.79 (19)	1.66–4.6	3.61	2.14–4.87	8.62	4.86–11.9
202	1.94 (62)	0.89–4.2	0.42	0.07–1.35	0.31	0.06–1.18
203	0.54 (78)	0.26–1.13	0.08	0.02–0.22	0.08	0.02–0.23
204	3.10 (49)	1.94–4.96	0.56	0.14–1.29	0.84	0.2–2.0
205	2.66 (52)	1.57–4.49	8.1	2.18–17.45	8.42	2.25–18.2
206	5.59 (52)	3.35–9.33	2.78	1.35–4.47	4.51	2.11–7.48
207	1.48 (109)	0.91–2.4	2.91	2.28–4.18	2.83	2.22–4.06
208	0.014 (96)	0.0053–0.039	0.01	0.006–0.016	0.01	0.007–0.019
209	1.78 (92)	1.16–2.73	2.79	1.21–4.25	5.51	2.24–8.65
210	7.1 (109)	4.68–10.78	2.74	2.33–4.57	2.36	2.01–3.9
211	0.29–0.71 (8–81)	0.194–1.15	0.28	0.26–0.39	0.37	0.34–0.51

The range (mean ± 1 standard deviation) shows skewness because the standard deviation depends on a logarithmic relation. At site 211, several separate wind-speed runs were made to determine the mean aerodynamically derived roughness length; the mean for each of these experiments ranged from 0.29 to 0.71 cm. For z_{o}^{A}, three collapsible 9.2-m-high wind towers were operated simultaneously at these sites each recording 1-min average wind speeds from three to four calibrated anemometers. The number of average wind speed values used to calculate z_{o}^{A} at each site is within the parentheses next to mean z_{o}^{A} value calculated for each site. Hourly thermal-gradient data from the nearest of two stations were extrapolated into 5-min intervals from which the time of thermal neutrality was inferred. Wind data within ± 60 min of the neutral time was considered valid for the calculation of z_{o}^{A} provided the wind speed at 9.2 m was not below 4 m s^{-1}. During these morning and evening periods, the temperature gradient generally remained less than ± 0.05 °C. Site 211 shows results derived for two different periods of thermal neutrality: one used only 8 data points, the other used 81 data points.

the height of the tallest roughness element in the Raupach model is always the best choice when multiple roughness elements of different heights are present. On the other hand, multiple roughness elements could be considered as one composite element whose height is equal to the tallest element.

The greatest disparities in the comparison of the aerodynamic and modeled roughness lengths may be attributed to: (1) local inhomogeneities in the wind field and errors in uniform instrument response, (2) inadequate documentation of the physical dimensions and distributions of non-erodible roughness elements, (3) inadequate estimates of drag coefficients and wind-stress non-uniformity, and (4) inadequacies in the roughness-length models. More work needs to be done to test the functional form of the friction velocity ratio model as described by Eqs. (10) and (11) and the roughness length models as described by Eqs. (19) and (20); a much better method is needed to determine the roughness parameters associated with porous objects.

An important result is that the individual threshold friction velocity ratios (R_i) for sites characterized by annual plants and grasses (sites 200–201, 202, 203, 209; Table 1) and the low-height "borage" (site 205) generally show values equal to or less than the values for the other sites. At site 204, the modeled roughness lengths were much lower than the aerodynamically measured roughness length, possibly because the roughness properties of annual plants there were not measured and included in the models.

Where present, therefore, the annual plants appear to play a major role in sheltering ground surfaces relative to the other species at a site. The presence or absence of the annual vegetation produces large variations in the model-derived sheltering. For example, removing the roughness contribution of the annuals from site 200 to site 201 diminishes the model-derived roughness length from approximately 6 cm (Table 2) to 5.2×10^{-4} cm. The latter roughness length is only slightly higher than those of the bare surfaces (1×10^{-5} cm) described by Marticorena et al. (1997) or used in this paper (4×10^{-4} cm). In terms of the threshold friction velocity, the annual plants produce a value 4.3 times higher than that produced by the bare surface, whereas the threshold friction velocity with the annual plants removed is only 1.4 times higher than the friction velocity of the bare surface. Such variability in the leafy vegetation of a species suggests that any measurements or estimates of roughness must account for all the roughness elements and the drag properties of each species present. Our models show this dramatic dependency in sheltering (magnitude of z_o) through the drag coefficient ratio, β. As an example, relatively minor leaf drop or breaking of stems following a period of drought dramatically increase the vulnerability of surfaces to wind erosion. Two related parameters, m (non-uniformity factor of wind stress) and C_d (drag coefficient of roughness species) in Raupach et al. (1993) basic model and in our extended model need a more physically based connection to roughness-element parameters than has been developed.

The importance of annual plants and of related interannual climatic variability is underscored by monitoring observations in the study area. We have monitored this area since autumn 1999 for sand movement, dust emission, meteorological phenomena, and vegetation change. Densest and highest vegetation characterized the area during spring 2001 compared to the preceding and following spring seasons. The extent of vegetation was closely related to rainfall during the prior 3-month periods. The January–February–March precipitation for 2001 was about 75 mm, in contrast to 20 mm for this period in 2000 and 6 mm in 2002. Analyses of wind speed and associated sand-flux data acquired from two permanent stations near our z_o-measurement sites show higher values of sand flux during spring 2000 than spring 2001 for similar forcing wind speeds. This relation indicates that the surface had a lower threshold friction velocity during spring 2000 than it did during spring 2001. The observed increase in plant cover, including annual vegetation, in the study area over this period is consistent with the observed changes in sand flux at the two monitoring stations. Relations among wind, dust emission, annual vegetation, and antecedent precipitation in the Sonoran Desert similarly show that antecedent precipitation induced germination and subsequent growth of annual plants that sheltered the surface during windstorms (MacKinnon et al., 1990).

Because z_o shows such a sensitive response to measured roughness geometry and drag coefficients, it would be useful to make more accurate field measurements of these properties employing some other method than measuring rods and tapes, such as automatically extracted parameters from remotely

sensed image data. For example, 20 cm (spatial resolution in width), stereo, color–infrared image data recently acquired for the Mojave study sites can resolve the width (w), height (h), and separation (D) parameters for bushes larger than a few tens of centimeters. Radar can also be used to obtain small-scale topographic roughness, such as coppice dunes, salt pushups, and surface clasts. The roughness properties of small annual plants are the most difficult to obtain directly by remote-sensing data, but change-detection methods using Landsat image data are capable of showing an integrated "greening" from these plants between dry and wet periods and thus give some indication of the presence, absence, and density of vegetation change. Airborne LIDAR may also be used to determine the heights and cover density of annual vegetation when the vegetation is relatively dense and can be distinguished from the ground. Remote-sensing methods may thus provide the means to obtain accurate and statistically significant measurements of surface roughness for environments that vary spatially and temporally.

Acknowledgements

We are grateful to two anonymous reviewers for their comments that greatly improved the manuscript. Frank Urban supplied meteorological data from the study area.

We are grateful to Rob Fulton (California Desert Studies Consortium, California State University at Fullerton) for logistical help. This work was supported by the Earth Surface Dynamics Program of the U.S. Geological Survey.

References

Arya, S.P.S., 1975. A drag partition theory for determining the large-scale roughness parameter and wind stress on Arctic pack ice. J. Geophys. Res. 80, 3447–3454.

Brutsaert, W., 1982. Evaporation into the Atmosphere: Theory, History, and Applications. D. Reidel Publishing, Boston. 299 pp.

Businger, J.A., Wyngaard, J.C., Izumi, Y., Bradley, E.F., 1971. Flux-profile relationships in the atmospheric surface layer. J. Atmos. Sci. 28, 181–189.

Conover, W.J., 1971. Practical Nonparametric Statistics. Wiley, New York. 462 pp.

Crawley, D.M., Nickling, W.G., 2003. Drag partition for regularly arrayed rough surfaces. Boundary-Layer Meteorol. 107, 445–468.

Gillette, D.A., 1988. Threshold friction velocities for dust production for agricultural soils. J. Geophys. Res. 93, 12645–12662.

Grant, P.F., Nickling, W.G., 1998. Direct field measurement of wind drag on vegetation for applications to windbreak design and modeling. Land Degrad. Dev. 9, 57–66.

Greeley, R., Iversen, J.D., 1985. Wind as a Geologic Process on Earth, Mars, Venus and Titan. Cambridge Univ. Press, New York. 333 pp.

Grell, G.A., Dudhia, J., Stauffer, D.R., 1995. A description of the fifth-generation Penn State/NCAR mesoscale model (MM5), NCAR Technical Note NCAR/TN-398+STR. 122 pp.

Lancaster, N., 1997. Response of aeolian geomorphic systems to minor climate change: examples from the southern California deserts. Geomorphology 19, 333–347.

Lee, J.A., 1990. The effect of desert shrubs on shear stress from the wind: an exploratory study. Unpublished PhD Thesis. Department of Geography, Arizona State University. 181 pp.

MacKinnon, D.J., Elder, D.F., Helm, P.J., Tuesink, M.F., Nist, C.A., 1990. A method of evaluating effects of antecedent precipitation on dust storms and its application to Yuma, Arizona, 1981–1988. Clim. Change 17, 331–360.

Marticorena, B., Bergametti, G., Gillette, D., Belnap, J., 1997. Factors controlling threshold friction velocity in semiarid and arid areas of the United States. J. Geophys. Res. 102 (D19), 23277–23287.

Musick, H.B., Trujillo, S.M., Truman, C.R., 1996. Wind-tunnel modeling of the influence of vegetation structure on the saltation threshold. Earth Surf. Processes Landf. 21, 589–605.

Raupach, M.R., 1992. Drag and drag partition on rough surfaces. Boundary-Layer Meteorol. 71, 211–216.

Raupach, M.R., Gillette, D.A., Leys, J.F., 1993. The effect of roughness elements on wind erosion threshold. J. Geophys. Res. 98 (D2), 3023–3029.

Raupach, M.R., 1994. Simplified expressions for vegetation roughness length and zero-plane displacement as functions of canopy height and area index. Boundary-Layer Meteorol. 71, 211–216.

Wolfe, S.A., 1993. Sparse vegetation as a surface control on wind erosion. PhD Dissertation, University of Guelph. 257 pp.

Wolfe, S.A., Nickling, W.G., 1996. Shear stress partitioning in sparsely vegetated desert canopies. Earth Surf. Processes Landf. 21, 607–619.

Wyatt, V.E., Nickling, W.G., 1997. Drag and shear stress partitioning in sparse desert creosote communities. Can. J. Earth Sci. 34, 1486–1498.

Yaglom, A.M., 1997. Comments on wind and temperature flux-profile relationships. Boundary-Layer Meteorol. 11, 89–102.